Local 2PPE-yield enhancement in a defined periodic silver nanodisk array

C. Wiemann [a,*], D. Bayer [a], M. Rohmer [a], M. Aeschlimann [a], M. Bauer [b]

[a] *Fachbereich Physik, Technische Universität Kaiserslautern, 67653 Kaiserslautern, Germany*
[b] *Institut für Experimentelle und Angewandte Physik, Christian-Albrechts-Universität Kiel, 24098 Kiel, Germany*

Abstract

Well-prepared periodic arrays of silver nanoparticles are investigated by means of linear and non-linear photoemission electron microscopy. The structures show homogeneous photoemission for UV excitation in the linear photoemission regime whereas striking inhomogeneities are mapped in the case of the nonlinear (2 photon) excitation using ultrashort 400 nm laser pulses. A detailed analysis enables to assign these inhomogeneities to defect induced electron momentum transfer processes only effective for the 2 photon excitation process. We propose this mechanism to be of relevance for the appearance of so-called hot spots in nonlinear photoemission as identified in other 2PPE studies in the past. Furthermore, the complementarity between all-optical studies and nonlinear photoemission studies of localized surface plasmons in nanoparticles is discussed.
© 2007 Elsevier B.V. All rights reserved.

Keywords: PEEM; 2PPE; Plasmon; Silver nanostructures

1. Introduction

Photoemission microscopy (PEEM) is a versatile tool for mapping the lateral distribution of photoelectrons generated at a structured surface. In combination with various methods of spectroscopy, a number of different contrast mechanisms can be exploited to gain information on the local electronic and chemical structure of the surface [1,2]. All spectroscopic methods combined with PEEM benefit from the fast parallel data acquisition which ensures a high degree of comparability of data taken at different locations inside the field of view. Recently, fs-laser induced nonlinear photoemission (NLPE) used in combination with PEEM has attracted considerable attention as a highly sensitive tool to surface properties obviously not accessible in conventional photoemission. For instance, Cinchetti et al. used 2 photon photoemission (2PPE) to map the lateral distribution of optical near fields in the vicinity of plasmon-resonant nanostructures [3]. Conventional threshold photoemission showed a completely different picture of the surface mapping the nanostructure topography. Another example is the appearance of distinct surface inhomogeneities (hot spots) in nonlinear photoemission as reported by various groups [4–7]. In many cases, these hot spots are completely absent in the PEEM image for threshold photoemission at irradiation with UV-light. A clear understanding of the underlying mechanisms is still lacking. One of the difficulties that have been met in the interpretation of these "hot spots" in the past is that the phenomenon of unusually high and strongly localized photoemission yield can originate from a number of different effects, among them field emission, thermal emission, and plasmon-enhanced photoemission.

The alternative contrast mechanisms in PEEM that are exclusively linked to the nonlinear photoemission process have the potential to open up complementary insights into

* Corresponding author.
  E-mail address: c.wiemann@fz-juelich.de (C. Wiemann).

the physics of nanostructured surfaces. However, for a reasonable interpretation of such data an improved understanding of the nonlinear photoemission process at nanostructured surfaces is required where not only the local optical field amplitude is considered but also the electronic band structure of the emitting material. As we will show for the case of metals, the response of the highly mobile conduction band electrons to an intense time-varying light field can open up additional pathways for photoemission which are not easily caught in the framework of standard one-step or three-step models. In the following, we particularly present experimental evidence for the relevance of defect structures acting as efficient momentum sources supporting nonlinear photoemission. An important prerequisite to identify the relevance of this mechanism in this work has been the use of periodic arrays of nanoparticles of well-defined size and shape.

2. Experimental

The PEEM used for our experiments is described in detail elsewhere [8]. Two different light sources are available to record PEEM images: a conventional mercury vapour UV source (high energy cut-off at 4.9 eV) and the frequency doubled output ($h\nu \approx 3.1$ eV) of a tuneable femtosecond Ti:sapphire laser system (760–840 nm wavelength range, 80 MHz repetition rate, 120 fs pulsewidth (FWHM)). The high peak intensities of the femtosecond pulses give rise to high nonlinear 2PPE-yields resulting in emission currents that are comparable to or even higher than those achieved in threshold photoemission with the mercury lamp. Our sample consists of a periodic array of silver nanodisks prepared by electron beam lithography (EBL) as described in reference [9]. In short, the structures were written into a polymethylmethacrylate (PMMA) resist layer deposited onto a glass plate substrate coated with a 30 nm thick semiconducting indium–tin–oxide (ITO) layer to prevent charging during the EBL process as well as during the photoemission experiment. After negative development, silver was evaporated onto the PMMA-mask at room temperature. The PMMA layer was then lifted from the substrate in an acetone bath, leaving only the written structure copied in silver (lift-off-process). By this means well-defined nanostructures are prepared, which have been widely used in the past to investigate for instance the decay dynamics of particle-characteristic plasmon modes in the time- as well as in the frequency-domain [10,11]. Fig. 1 shows a scanning electron micrograph (SEM) of the sample used in this study. The silver nanodisks have a diameter of 200 nm and a height of 50 nm. The optical properties of the nanodisk array were characterized by extinction spectroscopy through an optical microscope (Zeiss Axioskop with attached microspectrometer Zeiss MMS1). Afterwards, the sample was introduced into the vacuum chamber (base pressure: $1 \times 10E - 10$ mbar) that contains the photoemission microscope. During the transfer from the EBL system to the UHV chamber, the sample had to be exposed to air.
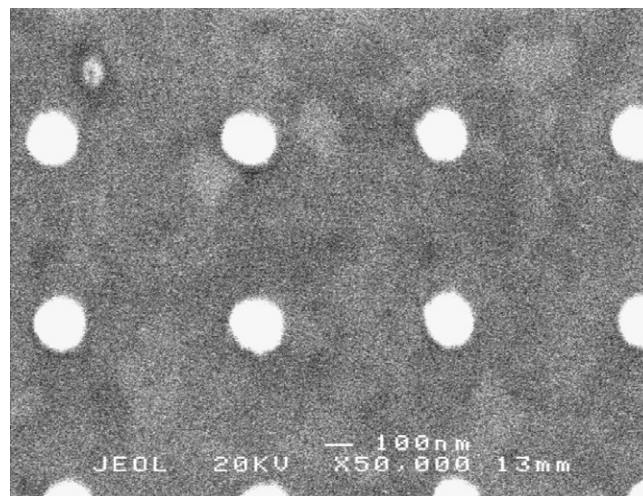

Fig. 1. SEM image of the periodic array of silver nanodots (diameter: 200 nm, height 50 nm, center-to-center distance 650 nm).

3. Results and discussion

Fig. 2 shows a PEEM image of the sample recorded using the UV-lamp. Image contrast in this threshold photoemission microscopy is primarily due to differences in the work function and the electron density of states of the different materials. The enhanced brightness of the silver nanodisks in comparison to the ITO-coated glass substrate is related to the higher density of occupied states near the Fermi level for the silver nanodisks which serve as initial states for the conventional photoemission process. The periodicity of the array pattern as well as the size of the nanodisks is imaged well, if the finite resolution of the emission microscope (<40 nm) is taken into account.
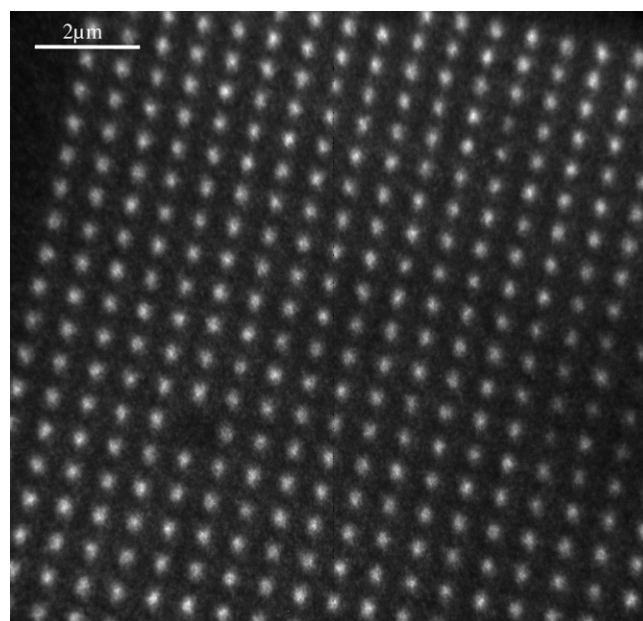

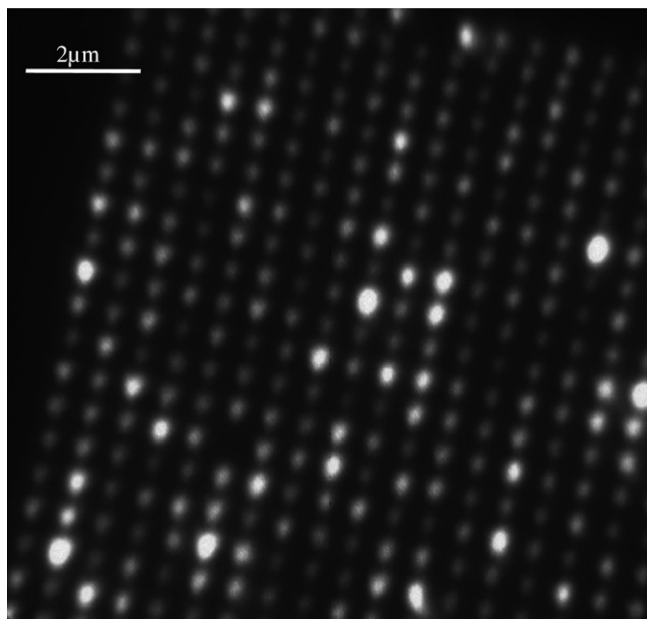Fig. 2. PEEM image of the sample recorded in threshold photoemission using the UV-light source (1PPE).

Fig. 3. 2PPE–PEEM image of the sample recorded using the second harmonic ($hv = 3.1$ eV) of the Ti:sapphire laser system.

As for the SEM image (Fig. 1) particle to particle variations in the electron emissivity are barely visible, indicating a very defined EBL preparation process throughout the periodic array.

A PEEM image recorded in the 2PPE-mode using the femtosecond laser source is shown in Fig. 3. Again, the periodicity of the array pattern is well resolved. However, in striking contrast to the UV-PEEM and the SEM image we observe large variations in the brightness values among the nanodisks. In comparison to Fig. 2, contrast enhancement as well as contrast reduction of individual particles with respect to the ITO substrate background is present. Some of the particles are almost hidden in the ITO background. The pronounced inhomogeneity in the 2PPE pattern is particularly interesting as past studies concerning the *optical* properties of such structures and performed at similar wavelength have shown a very homogeneous re-

sponse of the particle ensemble [12]. In recent publications inhomogeneities in the nonlinear photoemission of nanoparticles were assigned to particle to particle variations in the aspect ratio [6] and to variations in the particle orientation with respect to the direction of incidence or polarization of the exciting laser [7]. The approach used in the present work allows to explicitly exclude such effects. In contrast to self-organizing growth processes of the nanoparticles where the particle shape and size is governed to a large extent by the local environment of the substrate, the use of a lithography technique for the preparation of the nanoparticles in periodical arrays enables the preparation of particles with almost identical shape.

The analysis of brightness histograms as deduced from both 1PPE and 2PPE images enables a quantitative comparison of the observed contrast variations and give insight in the underlying mechanism responsible for the 2PPE from the nanodisks (see Fig. 4a and b). The histograms were obtained by averaging the brightness in both images over the same central area (size: 7×7 pixels) of each visible nanodisk. The relative width $\Delta I/\overline{I}$ of the brightness distribution is a measure of the inhomogeneity of the particle emissivity, where ΔI is the FWHM of the distribution and $\overline{I}$ is the average brightness of the particles. For the 2PPE process, we calculate a $\Delta I/\overline{I}$ value of about 2, which exceeds the corresponding 1PPE value of $\Delta I/\overline{I}$ of 0.15 by a factor of 13. Also obvious is the difference in the shape between the 1PPE and the 2PPE brightness distributions. The 1PPE histogram can be fitted rather well by a Gaussian distribution, whereas the 2PPE histogram is skewed and asymmetric. Next to the differences in the $\Delta I/\overline{I}$ value this gives further evidence that the 2PPE from the nanoparticles is governed by a different mechanism than the 1PPE process.

In the following, we will discuss potential mechanisms responsible for the differences in the characteristic 1PPE and 2PPE patterns. Based on the analysis of the histograms in Fig. 4a and b we will show that in contrast to the 1PPE the 2PPE relies on a momentum transfer process induced by local defects within the nanoparticles.
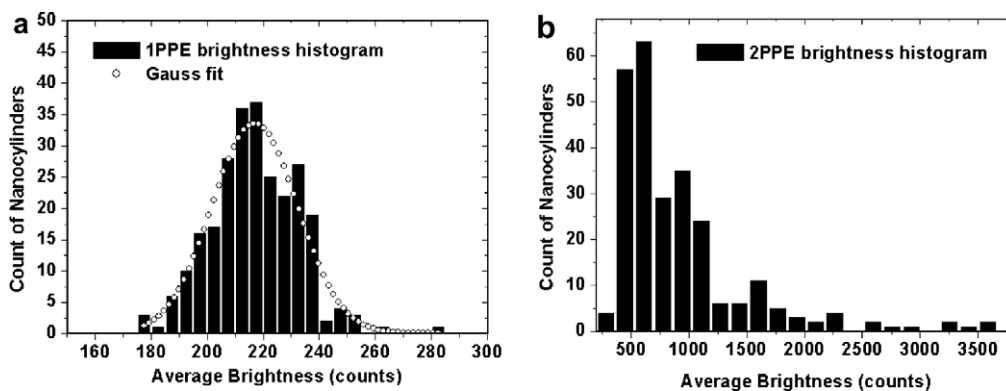

Fig. 4. Histograms of the average particle brightness derived from Figs. 2 and 3. The histograms were obtained by averaging the brightness in both images over the same central area (size: 7×7 pixels) of each visible nanodisk.

It is obvious that the imaged 2PPE inhomogeneities must be related to some inhomogeneity in the physical properties of the nanodisks. Particle to particle work function variations are *a priori* a very likely candidate in particular because the nanostructures had to be exposed to air during the required transfer from the EBL system to the PEEM chamber. An inhomogeneous contamination or even partly oxidation of the nanodisks' surface during the transfer will definitely affect the work function and consequently the contrast visible in the PEEM image. However, work function variations will affect both, 1PPE and 2PPE process, so that a corresponding inhomogeneity must be mapped in both images, Figs. 2 and 3. Even more, due to the smaller overall excitation energy in case of the 1PPE process (4.9 eV in comparison to 2×3.1 eV = 6.2 eV for 2PPE) the 1PPE emission is much closer to threshold and, therefore, more sensitive to work function variations. The lack of particle to particle inhomogeneities in the 1PPE image is therefore a proof that work function variations cannot account for the distinct 2PPE contrast. The identification of a particle intrinsic mechanism affecting exclusively the 2PPE process is obviously indispensable for a correct interpretation of Fig. 4.

For nanoscale silver crescents Cinchetti et al. could show that the photoemission microscopy patterns from 1PPE and 2PPE are indeed, governed by different contrast mechanisms [3]. Whereas the 1PPE images the topography of the crescent, the signal from the 2PPE process could be assigned to the electromagnetic near-field induced by excitation of the localized plasmon resonances (LSP or Mie-plasmon) in the vicinity of the silver nano-pattern. The high sensitivity of the 2PPE process to the near-field is attributed to the photon energy of the used laser system ($h\nu = 3.1$ eV), which lies close to the resonance energy of the Mie-plasmons in these silver nanostructures. The nanodisks investigated in the present study exhibit two different plasmon resonance energies corresponding to collective excitations of the conduction band electrons parallel or perpendicular to the substrate surface (parallel mode and perpendicular mode, respectively). Optical characterization of the sample by means of extinction spectroscopy at normal incidence determines the parallel mode resonance energy to be 1.8 eV. The experimental setup does not allow a direct access to the perpendicular mode spectrum, however, based on the Mie-theory approach a very reliable calculation of both resonance energies is possible [13]. Mie-theory gives exact solutions only for special geometries of the nanoparticle (spheroids). A number of approximate solutions to the problem have been suggested in the past. Among the simpler methods the quasi-static approximation is widely used, which is based on the assumption that the light field can be reasonably approximated by a homogeneous field, i.e., the wavelength is long compared to characteristic dimensions of the resonant structure [14]. Recently, Kuwata et al. have proposed an extension of the quasi-static model which includes the energy loss due to radiation (radiation damping or elastic scattering) as well as resonance shifts due to retar-

dation effects [15]. A simulation based on this model reveals two spectrally well separated resonances in the nanodisks as described above, one at 360 nm for excitation with the electrical field vector oriented along the cylinder axis (perpendicular mode) and a second at 690 nm for polarization perpendicular to the cylinder axis (parallel mode). The latter one was fitted to match the measured extinction spectrum by varying the dielectric constant of the surrounding medium, which is assumed to be real and independent of wavelength (see Fig. 5b). The thereby obtained numerical value of 1.28 for the dielectric constant of the surrounding medium is reasonable as it lies between the vacuum value and the real part of the ITO dielectric function, which is around 3 at the resonance wavelength of the parallel mode. The proximity of the perpendicular mode energy to the wavelength of the excitation light (≈ 400 nm) implies the possibility of near-resonant excitation conditions going along with a near-field contrast enhancement as monitored in the above mentioned experiment by Cinchetti et al. [3]. For the PEEM geometry (incidence angle: 65° with respect to the sample surface) this is possible using p-polarized laser light which exhibits a large component of the electric field vector parallel to the cylinder axis of the particle. In this context, inhomogeneities in the 2PPE response may arise from the well-known sensitivity of the LSP-resonance energy on the detailed geometry of a particle [16]. In the case of particle to particle variations in diameter or height, random shifts of the resonance wavelengths among the nanodisks in the array will emerge. That is, for a given photon energy only *some* of the nanodisks are excited resonantly. Only these selectively addressed nanoparticles will exhibit high near-field amplitudes accompanied by a high photoemission yield. The corresponding PEEM image would give rise to a random distribution of bright dots within the array similar to the 2PPE image in Fig. 3. However, at a different photon energy other nanodisks will be resonant and the visible PEEM pattern will change. 2PPE PEEM images recorded at different laser wavelength between 395 and 420 nm are shown in Fig. 5. Variations in the 2PPE response due to a potential inhomogeneous broadening of the plasmon resonance should easily be identified. However, the series of images in Fig. 5 exhibits only overall changes in the integral 2PPE intensity but no variations in the appearance of the 2PPE PEEM pattern from the array. We conclude that the particle to particle variations in the Mie resonance energy are much smaller than the homogeneous line width of the resonance and cannot account for the inhomogeneous 2PPE pattern. Calculations of extinction coefficients for varying particle diameters shown in Fig. 5b support this observation. The graph shows resonance curves for particles of 50 nm height and 190 nm, 200 nm and 210 nm diameter, respectively. At a homogeneous linewidth of the perpendicular mode of about 120 nm (FWHM) the resonance energy maximum varies by about 5 nm only. Note that SEM micrographs of the sample (see Fig. 1) indicate much smaller variations in the particle to particle diameter. This finding is also corrobo-
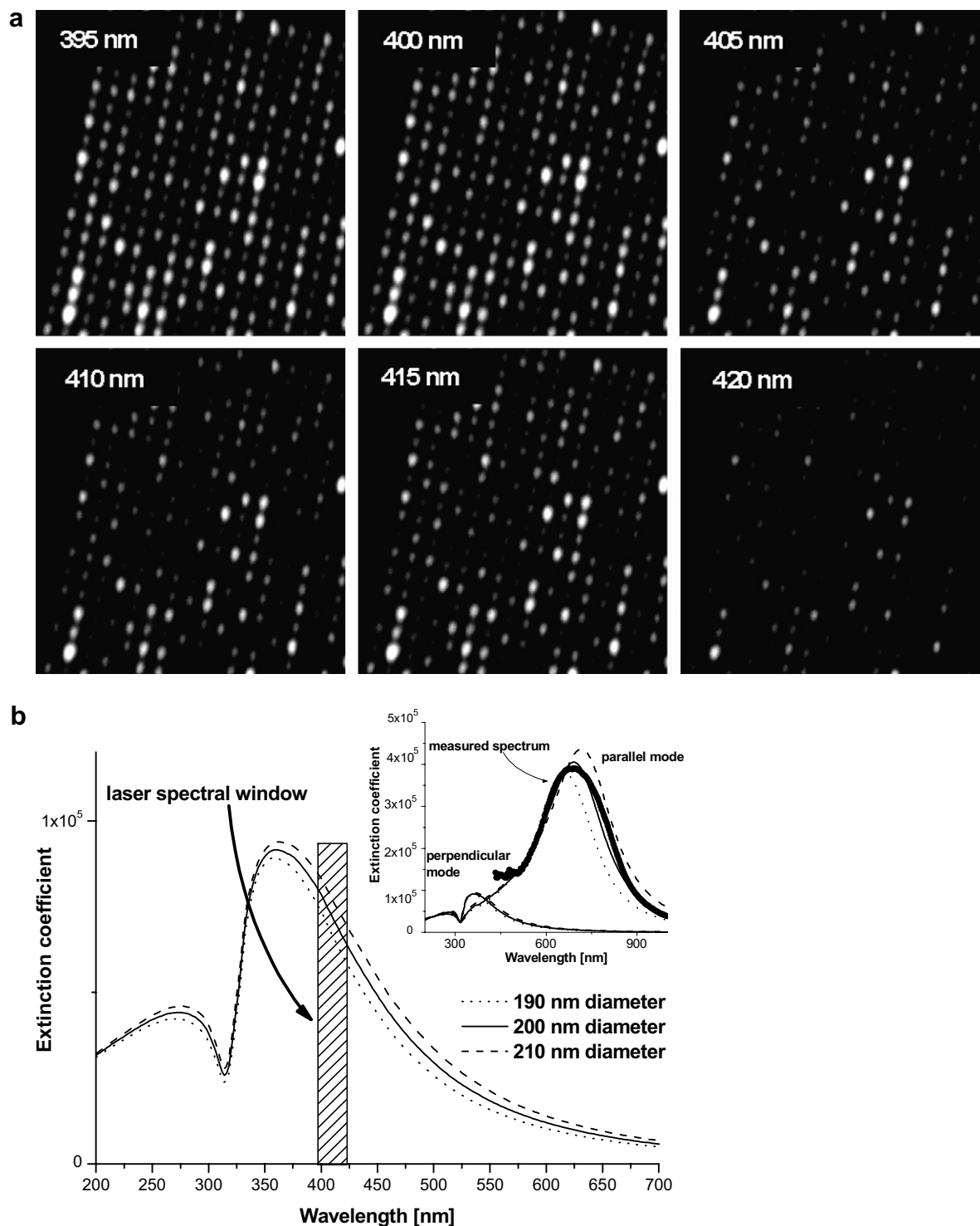
Fig. 5. (a) 2PPE–PEEM images recorded at different laser wavelengths as indicated in the insets. The overall brightness level is reduced due to the reduction of photon energy with increasing wavelength, while the relative brightness ratio between individual particles remains constant. (b) Calculated extinction spectra of the perpendicular plasmon mode for three different particle diameters (190, 200 and 210 nm). The shaded area corresponds to the experimentally accessible spectral tuning range. The inset shows the total calculated extinction spectra (perpendicular and parallel plasmon mode, thin lines) as well as the measured extinction spectrum (parallel mode, thick line).

rated by the results of all-optical experiments on the properties of the LSP-resonance of similarly prepared particle arrays, which have been performed in the time as well as in the frequency-domain. In these studies, no appreciable inhomogeneous broadening of the resonance was observed [12].
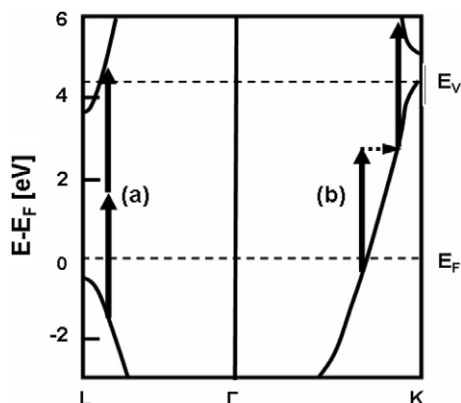
Fig. 6. Simplified band structure of bulk silver (following [16]). The arrows indicate possible optical transitions induced by 3.1 eV photons: (a) direct absorption via a virtual intermediate state and (b) indirect absorption via real intermediate states and involving momentum transfer scattering processes.

We finally conclude that the 2PPE brightness variations must originate from the two-step photoemission process itself. A close look to the band structure of silver [17] (see Fig. 6) highlights the possible pathways for the two-step excitation process at excitation by 3.1 eV photons. A direct (vertical) transition can take place between lower and upper sp-band near the L-symmetry point via simultaneous absorption of two photons. Alternatively, indirect transitions going along with intraband absorption along the gamma-K-direction are possible. While the direct transitions can take place only through simultaneous absorption of two photons involving a *virtual* intermediate state, the indirect transition leads to the transient population of a *real* intermediate state some eV above the Fermi level. Photoemission remains possible as long as a second photon is accepted within the lifetime of a few to some 10 fs [18] of the excited intermediate state. To account for momentum conservation the population of the intermediate state requires the involvement of a phonon [19] or, alternatively, a defect that breaks the crystalline periodicity of the solid, e.g. vacancies, impurities, displacements, or grain boundaries. These defects lift the restriction of momentum conservation connected to the translational invariance of the

crystalline lattice. In contrast, vertical transitions do not depend on additional momentum transfer and their probability is independent of the defect density. Therefore, a higher contribution of photoelectrons generated along the indirect pathway is to be expected if a high concentration of crystalline defects is present.

Is it possible to reproduce the measured intensity histogram of the 2PPE image under the assumption of defect-mediated 2PPE? If we think of generic crystalline defects being generated randomly during the evaporation step of the sample preparation, the probability of finding N defects in a given nanodisk is given as $p(N) = p(1)^N$, where $p(1)$ is the probability of generating a single defect. Such a probability distribution is shown in Fig. 7b in comparison to the measured 2PPE intensity histogram (Fig. 7a). Indeed, the qualitative coincidence of both graphs is rather striking. We take this as evidence that the observed inhomogeneity in the 2PPE brightness of the nanodisks originates from the random distribution of crystalline defects serving as scattering centres within the first step of the 2PPE process. The 2PPE–PEEM image obviously maps the defect density distribution throughout the nanodisk-array, with high defect concentrations appearing bright as they promote additional indirect transitions.

4. Conclusions

Lateral inhomogeneities in the nonlinear photoemission yield from single-crystalline as well as nanostructured surfaces have been observed in the past in numerous works [4–7]. The understanding of the underlying processes is therefore of high relevance for the interpretation of nonlinear photoemission data from surfaces in general. Already in these past works, the origin of hot spots has been assigned to the coupling of the light to defect structures [20]. In the present work, random defects acting as momentum sources in a two-step photoemission process could be determined to be the cause of the observed variations in the photoemission yield among otherwise homogeneously appearing nanoparticles. This was accomplished by making use of a comparative and quantitative analysis based on the brightness histograms deduced from 1PPE and 2PPE
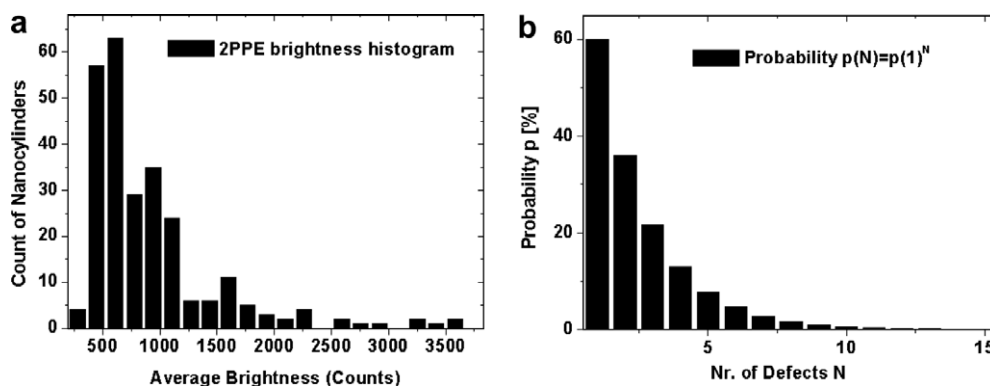

Fig. 7. Comparison of the 2PPE brightness histogram to a calculated defect probability distribution.

maps. An important ingredient in this context and contrary to former investigations was the use of well-prepared and rather defined periodic nanoparticle arrays, which is an indispensable precondition for the reliable interpretation of such histograms. A future step will be the identification of the relevant defect types. In this context, an interesting issue will be, for instance, the effective range of such defects in terms of a momentum source in photoemission. While crystalline defects and the resulting disturbance of the periodic lattice potential are localized on an atomic length scale, the wave functions of conduction band electrons in a metal extend over a much wider range. Therefore, promotion of indirect optical transitions by local defects may occur even at distances of some 10 nm. The lateral resolution as offered by PEEM is most likely not sufficient to resolve the defects that serve as sources of momentum transfer, but atomic resolution techniques such as STM will be required. A potential experimental approach enabling a direct access to the correlation between photoemission and atomic scale defect has been presented just recently in a combined STM/PEEM study of silver clusters on HOPG [21].

Finally, we would like to address a further point which is of relevance when comparing plasmon-resonant photoemission data of well-defined periodic nanostructures as presented in this work and corresponding all-optical studies by means of (lateral integrating) second harmonic generation and extinction spectroscopy. As mentioned above and in striking contrast to the observed inhomogeneities in the (plasmon mediated) 2PPE-yield distribution these latter studies revealed an almost homogeneous behaviour with respect to the investigated plasmon properties. We assign this seeming conflict between all-optical data and photoemission data to the intrinsic difference between these two complementary experimental approaches. In this context, it is important to be aware that a LSP excitation can only be sensed by its own decay. The decay of the LSP is mainly governed by two channels: the coupling to the propagating radiation field (radiation damping) and, alternatively, due to electron–hole excitations in or in the vicinity of the nanostructure (internal damping). With the exception of SNOM and related methods, optical methods rely on the information contained in the optical far-field, that is, on the coupling to the propagating radiation field as emitted by the plasmon in a radiative decay process [22]. In contrast, the photoemission process relies on the excitation of electrons that goes along with the internal damping [23]. It is a highly localized process and therefore governed by the near-field distribution induced by the plasmon excitation. Thus, photoemission and optical spectroscopy collect data from different energy loss channels while the overall damping rate of the plasmon resonance is determined by the sum of the individual rates of all contributing damping processes.

From the all-optical experiments it can be concluded that the scattering cross section, i.e., the ability of a particle to re-radiate energy into the far-field, does not vary consid-erably among the particles within an array. This reflects the homogeneity in particle size and geometry that can be achieved by EBL preparation, since these properties govern the rate of radiation damping. On the other hand, our 2PPE results show that electron emissivity varies strongly from one particle to the other. It maps directly variations in the efficiency of the internal damping of the plasmon resonance, i.e., the ability of the particle to convert energy from the radiation field to internal electron–hole excitations, which is governed by the inhomogeneity in the internal structure among the particles. As for the particle size regime studied here ($d > 50$ nm), radiation damping gives by far the strongest contribution to the total damping (about 98%). Inhomogeneities in the internal damping do effectively not transfer to inhomogeneities in the total damping rate of the plasmon resonance as determined for instance from linewidth analysis of extinction spectra because the total damping rate is dominated by radiation damping.

Acknowledgements

References

[1] M. Merkel, M. Escher, J. Settemeyer, D. Funnemann, A. Oelsner, C. Ziethen, O. Schmidt, M. Klais, G. Schönhense, Surf. Sci. 480 (2001) 196.

[2] G. Schönhense, J. Electron Speccstrosc. Relat. Phenom. 137 (2004) 769.

[3] M. Cinchetti, A. Gloskowskii, S.A. Nepjiko, G. Schönhense, H. Rochholz, M. Kreiter, Phys. Rev. Lett. 95 (2005) 047601.

[4] O. Schmidt, G.H. Fecher, Y. Hwu, G. Schönhense, Surf. Sci. 482–485 (2001) 687.

[5] M. Cinchetti, A. Oelsner, G.H. Fecher, H.J. Elmers, G. Schönhense, Appl. Phys. Lett. 83 (2003) 1503.

[6] G.H. Fecher, O. Schmidt, Y. Hwu, G. Schönhense, J. Electron Spectrosc. Relat. Phenom. 126 (2002) 77.

[7] L.I. Chelaru, M. Horn-von Hoegen, D. Thien, F.-J. Meyer zu Heringdorf, Phys. Rev. B 73 (2006) 115416.

[8] W. Swiech, G.H. Fecher, Ch. Ziethen, O. Schmidt, G. Schönhense, K. Grzelakowski, C.M. Schneider, R. Frömter, H.P. Oepen, J. Kirschner, J. Electron Spectros. Relat. Phenom. 84 (1997) 171.

[9] W. Gotschy, K. Vonmetz, A. Leitner, F.R. Aussenegg, Appl. Phys. B 63 (1996) 381.

[10] B. Lamprecht, J. Krenn, A. Leitner, F.R. Aussenegg, Phys. Rev. Lett. 83 (1999) 4421.

[11] B. Lamprecht, A. Leitner, F.R. Aussenegg, Appl. Phys. B 68 (1999) 419.

[12] B. Lambrecht, J.R. Krenn, A. Leitner, F.R. Aussenegg, Appl. Phys. B 69 (1999) 223.

[13] G. Mie, Ann. Phys. 25 (1908) 377.

[14] C.F. Bohren, D.R. Huffmann, Absorption and Scattering of Light by Small Particles, Wiley, New York, 1983.

[15] H. Kuwata, H. Tamaru, K. Esumi, K. Miyano, Appl. Phys. Lett. 83 (2003) 4625.

C. Wiemann et al. / Surface Science xxx (2007) xxx–xxx

[16] K.L. Kelly, E. Coronado, L.L. Zhao, G.C. Schatz, J. Phys. Chem. B 107 (2003) 668.

[17] K. Stahrenberg, T. Herrmann, et al., Phys. Rev. B 64 (2001) 115111.

[18] M. Aeschlimann, M. Bauer, S. Pawlik, Chem. Phys. 205 (1996) 127;
M. Merschdorf, C. Kennerknecht, W. Pfeiffer, Phys. Rev. B 70 (2004) 193401.

[19] E. Knösel, A. Hotzel, T. Hertel, M. Wolf, G. Ertl, Surf. Sci. 368 (1996) 76.

[20] M. Aeschlimann, C.A. Schmuttenmaer, H.E. Elsayed-Ali, R.J.D. Miller, J. Cao, Y. Gao, D.A. Mantell, J. Chem. Phys. 102 (1995) 8606.

[21] M. Rohmer, C. Wiemann, M. Munzinger, L. Guo, M. Aeschlimann, M. Bauer, Appl. Phys. A 82 (2006) 87.

[22] B. Lamprecht, G. Schider, R.T. Lechner, H. Ditlbacher, J.R. Krenn, A. Leitner, F.R. Aussenegg, Phys. Rev. Lett. 84 (2000) 4721.

[23] C. Sönnichsen, T. Franzl, T. Wilk, G. von Plessen, J. Feldmann, Phys. Rev. Lett. 88 (2002) 077402.